Journal of Alloys and Compounds 492 (2010) 378–383

Contents lists available at ScienceDirect

Journal of Alloys and Compounds

journal homepage: www.elsevier.com/locate/jallcom

Optical and structural properties of CuO nanofilm: Its diode application

İbrahim Y. Erdoğan [a], Ö. Güllü [b,*]

[a] Bingöl University, Faculty of Sciences and Arts, Department of Chemistry, 12000 Bingöl, Turkey
[b] Batman University, Faculty of Sciences and Arts, Department of Physics, 72060 Batman, Turkey

ARTICLE INFO

Article history:
Received 30 September 2009
Received in revised form
14 November 2009
Accepted 16 November 2009
Available online 20 November 2009

Keywords:
MIS diode
Nanofilms
CuO
Metal oxides
Schottky barrier
Band gap

ABSTRACT

The high crystalline CuO nanofilms have been prepared by spin coating and annealing combined with a simple chemical method. The obtained films have been characterized by X-ray diffraction (XRD), Fourier transform infrared (FT-IR) spectroscopy, ultraviolet–vis (UV–vis) spectroscopy and photoluminescence (PL) spectroscopy. Structural analysis results demonstrate that the single phase CuO on Si (1 0 0) substrate is of high a crystalline structure with a dominant in monoclinic (1 1 1) orientation. FT-IR results confirm the formation of pure CuO phase. UV–vis absorption measurements indicate that the band gap of the CuO films is 2.64 eV. The PL spectrum of the CuO films shows a broad emission band centered at 467 nm, which is consistent with absorption measurement. Also, Au/CuO/p-Si metal/interlayer/semiconductor (MIS) diodes have been fabricated. Electronic properties (current–voltage) of these structures were investigated. In addition, the interfacial state properties of the MIS diode were obtained. The interface-state density of the MIS diode was found to vary from 6.21×10^{12} to 1.62×10^{12} eV^{-1} cm^{-2}.

1. Introduction

Metal oxide nanostructures, as promising materials, have attracted much attention because of their extraordinary properties in different fields of optics, optoelectronics, catalysts, biosensors and so on. In this regard, copper oxide-based materials with nanostructures have been widely investigated due to their potential applications in chemical, photochemical and electrochemical fields, particularly in water splitting under visible light irradiation, windows for solar energy conversion and catalytic as well as electrochromic applications [1–6].

CuO is a promising semiconductor material for solar cell fabrication due to its suitable optical properties [3,5]. Furthermore, it is attractive as a selective solar absorber since it has a high solar absorbency and a low thermal emittance [6]. Copper oxide films have been reported to show native p-type conductivity due to copper vacancies in the structure. An important advantage of using CuO in device applications is that it is non-toxic and its constituents are available in abundance [3].

There has been considerable interest in the experimental studies of metal-semiconductor (MS), metal-interlayer-semiconductor (MIS) type Schottky diodes in the past decades [7–9]. The popularity of such studies is rooted in their importance to the interlayer between metal and semiconductor. Because the performance and reliability of these devices is especially dependent on the formation of interlayer, they strongly influence the device parameters, such as the interface-state density, Schottky barrier height (SBH) and ideality factor [8,9]. The electrical parameters of MS structures can be modified by interfacial layer when an interlayer is inserted between the semiconductor and metal. The studies made in literature have shown that the barrier height could be either increased or decreased by using an interlayer on the semiconductor substrate [10–18]. The new electrical properties of the MS contacts can be promoted by means of the choice of suitable interlayer [10]. For example, Gupta et al. [15] have recently reported the effect of temperature on diode parameters of Au/Cu_2O/p-Si heterojunction. They [15] have fabricated Cu_2O/p-silicon Schottky junction by using the pulsed laser deposition technique. Gupta et al. [15] have characterized the deposited Cu_2O film by using the X-ray diffraction technique, UV–vis spectroscopy, and electrical method. They [15] have reported that the Cu_2O film was amorphous in nature with optical band gap of 2.2 eV. Also, temperature dependence of current–voltage characteristics of Cu_2O/p-silicon Schottky junction has been studied in the range 200–300 K [15]. They [15] have found that the junction parameters such as ideality factor and barrier height were estimated by using the thermionic emission model. Gupta et al. [15] have observed that barrier height increased with the increase in temperature while ideality factor decreased with temperature.

In this paper, the optical and structural properties of the CuO films deposited on p-Si substrates by the spin coating method have been investigated by the ultraviolet-visible (UV–vis) spectroscopy,

* Corresponding author. Tel.: +90 488 213 2782; fax: +90 488 215 7201.
E-mail address: omergullu@gmail.com (Ö. Güllü).

0925-8388/$ – see front matter © 2009 Elsevier B.V. All rights reserved.
doi:10.1016/j.jallcom.2009.11.109

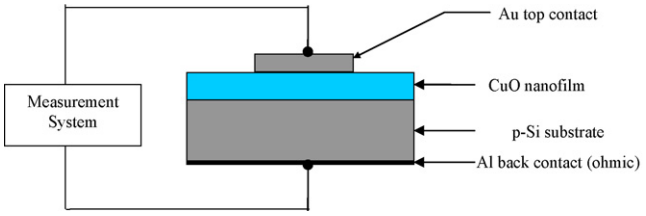

Fig. 1. The schematic structure of the Au/CuO/p-Si MIS device.

Fourier transform infrared (FT-IR) spectroscopy, photoluminescence (PL) spectroscopy and X-ray diffraction method (XRD). Also, we have studied the electrical properties of the Au/CuO/p-Si MIS diode structure (see Fig. 1). To our knowledge, no information is available in the literature on the electronic device properties of Au/CuO/p-Si MIS diode.

2. Experimental details

2.1. Preparation of CuO nanofilms

The dispersions of CuO particles prepared via a simple chemical method [19] have been spin coated and annealed on Si (1 0 0) substrates. This chemical method makes use of a 0.1 M $Cu(NO_3)_2$ (Aldrich 99.999% purity) solution with a 0.05 M NaOH (Aldrich 99.999% purity) solution. The p-type Si (1 0 0) wafer has been chemically cleaned using the RCA cleaning procedure (i.e., 10 min boil in $NH_3 + H_2O_2 + 6H_2O$ followed by a 10 min $HCl + H_2O_2 + 6H_2O$ at 60 °C temperature) before making deposition and contacts. Stock solutions of $Cu(NO_3)_2$ and NaOH have been prepared by dissolving $Cu(NO_3)_2$ and NaOH in deionized water (resistivity > 18 MΩ cm). NaOH solution has been added drop by drop in $Cu(NO_3)_2$ solution under magnetic stirring condition. The solutions have been mixed in a ratio of 1:1 at room temperature. Addition of NaOH solution to $Cu(NO_3)_2$ solution produces a blue color precipitate of $Cu(OH)_2$ as indicated in Eq. (1).

$$Cu(NO_3)_2 + 2NaOH \rightarrow Cu(OH)_2 + 2NaNO_3 \quad (1)$$

This blue color $Cu(OH)_2$ has been heated at 90 °C for an hour. Heating of the precipitates helps in better crystallization of materials and in the formation of particles of CuO as shown in Eq. (2).

$$Cu(OH)_2 \rightarrow CuO + H_2O \quad (2)$$

The as-obtained black color precipitates have been washed with deionized water and dried. The black color precipitate is an indication of the formation of CuO. The dried CuO particles have been dispersed in nonpolar organic solvents such as hexane or toluene. The dispersions have been added onto the Si substrate with a pipette. The substrates have been spin coated at 1000 rpm and then accelerated to the final rotation speed. The final rotation speed has been adjusted 3000 rpm for 20–30 s. After coating, the samples have been annealed in oxygen atmosphere at 350 °C for 2 h. The annealing treatment is widely known as a conventional and an effective technique to improve the crystalline quality [20–25]. In other words, the annealing process generally crystallizes the film structure. XRD studies as stated in the following sections display that as-deposited films have the weak crystal orientation or amorphous structure. After application of the annealing process, the CuO film with weak crystal orientation crystallizes to monoclinic phase that has prominent diffraction peaks. There are some works that support this case [20–25]. For example, Caglar et al. [25] have recently reported that ZnO films could be fabricated by a sol–gel spin coating on (1 0 0) p-type silicon substrates. They [25] have demonstrated that the heat treatment could modify the crystal structure, grain growth kinetics and orientation properties of the ZnO nanofilm. The thickness of the CuO thin films has been approximately measured as 80 nm by a gravimetric weight difference method [26].

2.2. Characterization of the CuO nanofilms

FT-IR transmission spectra of the deposited CuO films on Si substrates have been measured by using a PerkinElmer Spectrum One FT-IR spectrometer in the spectral range of 300–800 cm^{-1} at room temperature. The absorbance spectra of deposited CuO nanofilms have been measured by using a PerkinElmer Lambda 35 model UV–vis spectrophotometer in the spectral range of 300–800 nm at room temperature. The PL spectra have been measured at room temperature by using a Shimadzu RF-5301 PC Spectrofluorophotometer. XRD experiments for CuO films on Si (1 0 0) were performed in a Rigaku advance powder X-ray diffractometer instrument using Cu Kα radiation (λ = 1.5405 Å), operating at 30 kV and 30 mA over a 2θ range of 20–70°. The XRD phases present in the deposits were identified with the help of the JCPDS-ICDD.

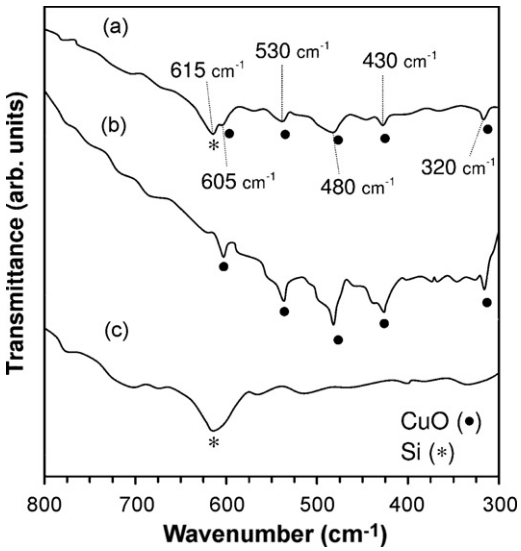

Fig. 2. The FT-IR spectra of CuO films deposited on Si substrate (a) dried CuO powder (b) and Si (c).

2.3. Fabrication and electronic characterization of Au/CuO/p-Si MIS diodes

After the deposition of CuO nanofilms on p-Si substrates with Al ohmic contact, Au metal contact was evaporated on CuO nanofilm by a vacuum coating unit at about 10^{-5} mbar. Diameters of Au dots were 1.0 mm (diode area = 7.85×10^{-3} cm^2). Current–voltage (*I–V*) measurement was taken by using a Keithley 487 Picoammeter at room temperature and in dark conditions (see Fig. 1).

3. Results and discussion

3.1. Characterization of the CuO nanofilms on p-Si substrate

The FT-IR transmission spectra recorded and shown in Fig. 2 also confirm the formation of CuO phase. The FT-IR spectrum (Fig. 2(a)) of spin coated and annealed CuO on Si consists of peaks at 320, 430, 480, 530, 605 and 615 cm^{-1}, approximately. The peaks at 320, 430, 480, 530 and 605 cm^{-1} correspond to characteristic stretching vibrations of Cu–O bond in the CuO [27,28]. The peak at 615 cm^{-1} can belong to Si or Cu_2O [29]. For characterization of peak at 615 cm^{-1}, FT-IR spectra of dried CuO powder (in KBr) and Si substrate have been recorded and shown in Fig. 2(b) and (c), respectively. These results confirm the formation of pure CuO phase on Si (1 0 0) substrate.

Optical absorption of the CuO nanofilm on p-Si substrate was analyzed by the following relationship,

$$\alpha h\nu = B(h\nu - E_g)^m, \quad (3)$$

where *B* is a constant, E_g is the optical band gap, α is absorption coefficient of the film, which was calculated from the optical absorbance (*A*) of the film according to $A = 0.434\alpha d$ [30]. The exponent *m* depends on the nature of the transition, *m* = 1/2, 2, 3/2, or 3 for allowed direct, allowed non-direct, forbidden direct or forbidden non-direct transitions, respectively. The absorption ($\alpha \geq 10^4$ cm^{-1}) is related to direct band transitions [31–33]. Fig. 3(a) shows optical absorption spectrum of the CuO thin film on p-Si substrate. Fig. 3(b) shows the plot of $(\alpha h\nu)^2$ *vs.* $h\nu$ according to Eq. (1). Satisfactory fit is obtained for $(\alpha h\nu)^2$ *vs.* $h\nu$ indicating the presence of a direct band gap [32,33]. The optical energy gap of the CuO film was determined as 2.64 eV by extrapolating the linear portion of this plot at $(\alpha h\nu)^2 = 0$ which indicates that the direct allowed transition dominates in the CuO film. This band gap energy value is consistent with that of 2.60 eV reported by Liu et al. [34] and that of 2.75 eV reported by Zhang et al. [35].

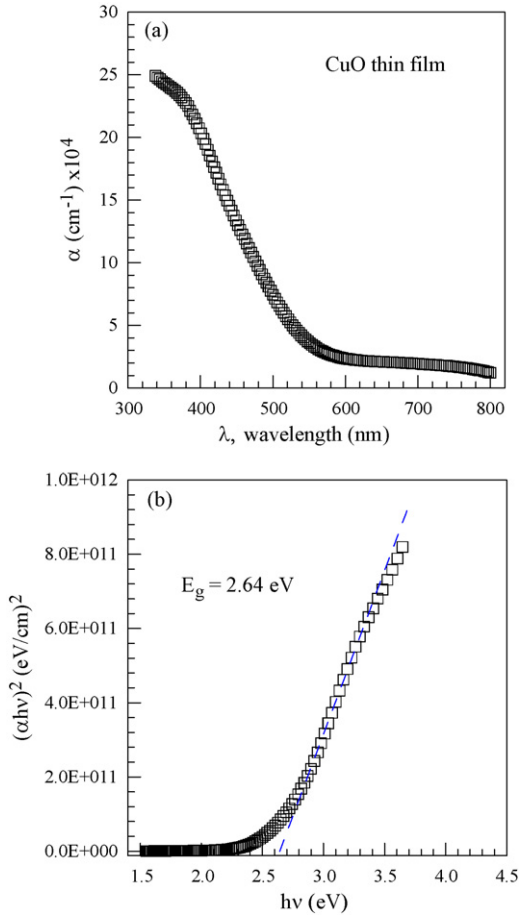

Fig. 3. The plots of (a) absorption and (b) $(\alpha h\nu)^2$–$h\nu$ of CuO nanofilm on p-Si substrate.

The emission properties of the CuO films have been studied at room temperature by using a PL spectrum excited with a 335 nm. PL study is a powerful tool to investigate the optical properties of semiconductor metal oxides. The room temperature PL spectrum of CuO films is shown in Fig. 4. The PL spectrum of the CuO shows a broad emission band centered at 467 nm (2.66 eV), which is consistent with absorption measurement. This broad blue range emission peak is attributed to the near-band-edge emission. Similarly, Kim and co-workers [36] have indicated that the emission peak of the

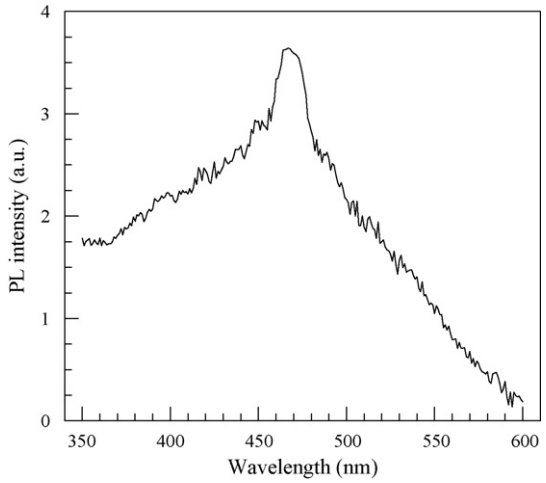

Fig. 4. The PL spectrum of CuO films on Si substrate.

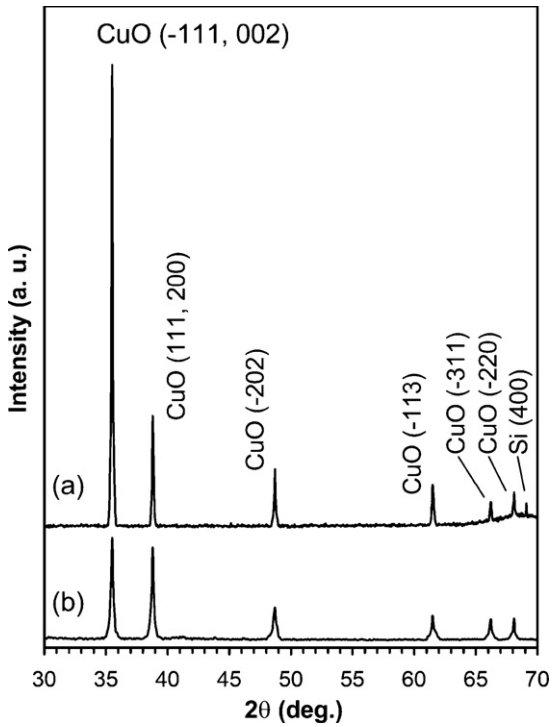

Fig. 5. The XRD patterns of CuO nanofilms on Si substrate (a) and dried CuO powder (b).

PL spectrum for CuO nanoparticles is observed in the blue region. The PL emission of the CuO films shifts shorter wavelength in comparison with that of the reported value for bulk band gap of CuO [37], which could arise from the quantum confinement effect.

The structural analysis of CuO nanofilms has been carried out by XRD and the evolved diffraction peaks could be indexed to a monoclinic phase of CuO and the lattice parameters have been obtained as $a = 4.68$, $b = 3.42$, $c = 5.13$ and $\beta = 99.5$ (JCPDS-ICDD 05-0661, 13-0420, 45-0937, 48-1548). The standard card pertained to Si is JCPDS-ICDD 27-1402. The XRD pattern of the CuO films prepared by spin coating and annealing process on Si substrate is shown in Fig. 5(a). To estimate the quality of the thin film data, XRD diffractogram of dried CuO powder for better comparison has been recorded and shown in Fig. 5(b). The XRD diffractogram of spin coated and annealed CuO film consists of a single strong diffraction peak at 35.5° (2θ scale) arising from (−1 1 1 and 0 0 2) reflections of monoclinic phase CuO. The weak peak at 69.1° corresponds to (4 0 0) reflection of Si, which belongs to substrate in this work. The other weak diffractions at 38.8°, 48.7°, 61.5°, 66.2°and 68.1° correspond to (1 1 1 and 2 0 0), (−2 0 2), (−1 1 3), (−3 1 1) and (−2 2 0) reflections of CuO. This case indicates that the crystallites in the CuO film as different from CuO powder have a preferred growth in this direction and the all peaks belong to single phase CuO. The (−1 1 1) reflection of CuO give full width at half maximum value of 0.11°. These results indicate that highly crystalline films of CuO can be grown at kinetically preferred orientation on Si (1 0 0) substrate.

3.2. Analysis of current–voltage characteristic of the Au/CuO/p-Si MIS structure

Fig. 6 shows the experimental semi-log I–V characteristic of the Au/CuO/p-Si MIS Schottky device at room temperature. As clearly seen from Fig. 6, the Au/CuO/p-Si Schottky structure is rectifying. The weak voltage dependence of the reverse-bias current and the exponential increase of the forward bias current are the characteristic properties of rectifying contacts. The current curve in

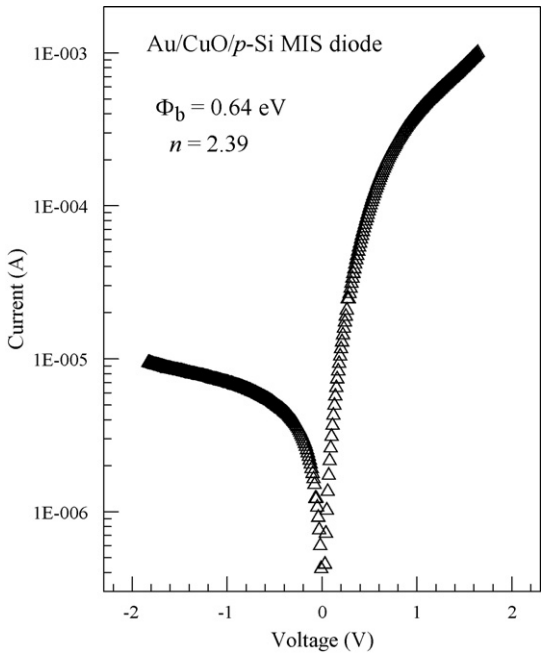

Fig. 6. Current–voltage characteristic of the Au/CuO/p-Si MIS diode.

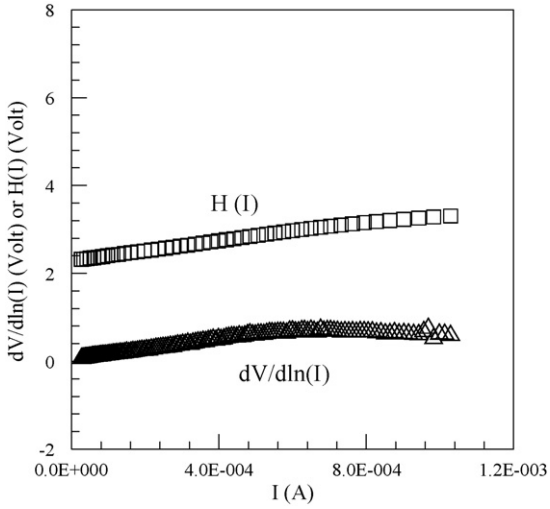

Fig. 7. $dV/d\ln I$ *vs. I* and $H(I)$ *vs. I* plots obtained from the experimental *I–V* data in Fig. 6.

forward bias region becomes dominated by series resistance from contact wires or bulk resistance of the CuO layer and p-Si semiconductor, giving rise to the curvature at high current in the *I–V* plot. By using thermionic emission (TE) theory [7,38], the ideality factor (n) and BH (Φ_b) can be obtained from the slope and the current axis intercept of the linear region of the forward bias *I–V* plot, respectively. The values of the BH and the ideality factor for the Au/CuO/p-Si diode have been calculated as 0.64 eV and 2.39, respectively. The ideality factor determined by the image-force effect alone should be close to 1.01 or 1.02 [39–41]. Higher values of ideality factors are attributed to secondary mechanisms which include interface dipoles due to interface doping or specific interface structure as well as fabrication-induced defects at the interface [39–42]. According to Tung [41], the large values of n may also be attributed to the presence of a wide distribution of low-Schottky barrier patches caused by laterally barrier inhomogeneous. Also, the image-force effect, recombination-generation, and tunneling may be possible mechanisms that could lead to an ideality factor value greater than unity [38].

Φ_b value of 0.64 eV that we have obtained for the Au/CuO/p-Si MIS device with CuO interlayer is remarkably higher than that achieved with conventional MS contacts such as Au/*p*-Si diode, where Φ_b is about 0.50 eV [7]. In literature, some studies have made experimentally for the barrier height modification using the interlayer films [43]. Recently, Temirci and Çakar [44] have published a paper about Cu/Rhodamine-101/p-Si/Al diode with height value of 0.78 eV and ideality factor value of 1.54. The obtained barrier height value of the diode is higher than the conventional Cu/p-Si [7]. In other study, Karataş et al. [45] have fabricated Al/Rh101/p-Si/Al contact. The barrier height (0.817 eV) of the Al/Rh101/p-Si/Al contact is significantly larger than the barrier height of conventional Al/p-Si Schottky diode. In another study, Çakar et al. [46] have fabricated the Cu/pyronine-B/p-Si, Au/pyronine-B/p-Si, Al/pyronine-B/p-Si and Sn/pyronine-B/p-Si diodes, and the obtained barrier heights for these diodes are larger than the conventional metal/p-Si contact. They [46] have evaluated that the barrier height could be enhanced or modified by using the thin interfacial films. It is seen from the above results that the interlayer can be used to vary the effective barrier height of metal/p-Si Schottky diodes. Furthermore, this case may be ascribed to the interlayer modifying the effective barrier height by influencing the space charge region of the inorganic substrate [47–50]. The CuO interlayer forms a physical barrier between Au metal and the p-Si wafer. This interlayer can produce substantial shift in the work function of the metal and in the electron affinity of the semiconductor and in turn, the interlayer gives an excess barrier of 0.14 eV, i.e., the CuO interlayer increases the barrier height of Au/p-Si. The barrier height of Au/p-Si contact increases by the insertion of a dipole layer between p-Si semiconductor and CuO interlayer. Similarly, Zahn et al. [51] have indicated that the initial increase or decrease in effective barrier height for the organic interlayer is correlated with the energy level alignment of the lowest unoccupied molecular orbital with respect to the conduction band minimum of the inorganic semiconductor at the organic/inorganic semiconductor interface. As a result, we have evaluated that Au/p-Si MS diode could be designed to exhibit the desired properties by means of the choice of the interlayer [43].

It is well known that the downward concave curvature of the forward bias current–voltage plots at sufficiently large voltages is caused by the effect of series resistance (R_s), apart from the interface states, which are in equilibrium with the semiconductor [52]. The R_s values have been calculated by using a method developed by Cheung and Cheung [53,54]. According to Cheung and Cheung [54], the forward bias *I–V* relation of a MIS diode with the series resistance can be expressed as:

$$I = I_0 \exp\left[\frac{q(V - IR_s)}{nkT}\right], \tag{4}$$

where IR_s term is the voltage drop across series resistance of device. The values of the series resistance can be determined from following functions by using Eq. (4);

$$\frac{dV}{d(\ln\ I)} = \frac{nkT}{q} + IR_s, \tag{5}$$

$$H(I) = V - \left(\frac{nkT}{q}\right)\ln\left(\frac{I}{AA^*T^2}\right), \tag{6}$$

and $H(I)$ is given as follows:

$$H(I) = n\Phi_b + IR_s, \tag{7}$$

A plot of $dv/d(\ln 1)$ *vs. I* will be linear and gives R_s as the slope and nkT/q as the *y*-axis intercept from Eq. (5). Fig. 7 shows a plot of $dv/d(\ln 1)$ *vs. I* at room temperature. The values of n and R_s have

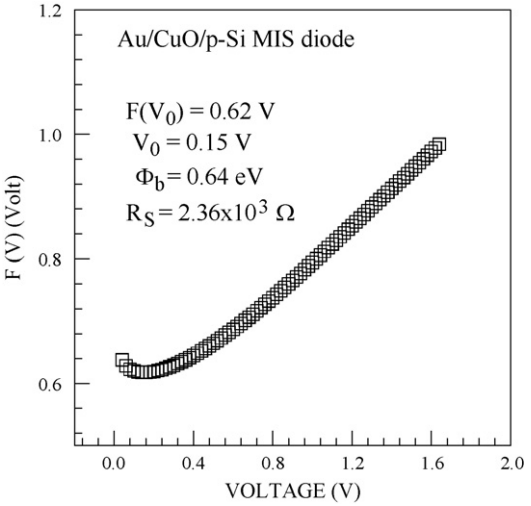

Fig. 8. *F*(*V*) *vs. V* plot obtained from the experimental *I–V* data in Fig. 6.

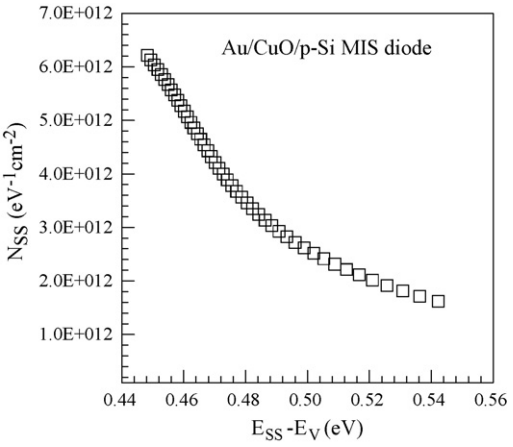

Fig. 9. N_{SS} *vs.* $(E_{SS} - E_V)$ plot of the Au/CuO/p-Si MIS device.

been calculated as $n = 3.82$ and $R_s = 1.14 \times 10^3\ \Omega$, respectively. It is observed that there is a large difference between the value of n obtained from the forward bias ln *I–V* plot and that obtained from the $dV/d(\ln I) - I$ curve (see Fig. 7). This may be attributed to the existence of the series resistance and interface states and to the voltage drop across the interfacial layer (native oxide plus CuO interlayer) [55].

Besides, *H*(*I*) *vs. I* plot have to be linear according to the Ref. [54]. The slope of this plot gives a different determination of R_s. By using the value of the n obtained from Eq. (5), the value of Φ_b is obtained from the *y*-axis intercept. *H*(*I*) *vs. I* curve is shown in Fig. 7. From *H*(*I*) *vs. I* plot, Φ_b and R_s have been calculated as 0.61 eV and $1.05 \times 10^3\ \Omega$, respectively.

Norde proposed an alternative method to determine value of the series resistance [56]. The following function has been defined in the modified Norde's method:

$$F(V) = \frac{V}{\gamma} - \frac{1}{\beta}\ \ln\left(\frac{I(V)}{AA^*T^2}\right) \tag{8}$$

where γ is an integer (dimensionless) greater than n. $I(V)$ is current obtained from the *I–V* curve and β is a temperature-dependent value calculated with $\beta = q/kT$. Once the minimum of the *F* vs. *V* plot is determined, the value of barrier height can be obtained from Eq. (9),

$$\Phi_b = F(V_0) + \frac{V_0}{\gamma} - \frac{kT}{q} \tag{9}$$

where $F(V_0)$ is the minimum point of $F(V)$ and V_0 is the corresponding voltage.

Fig. 8 shows the *F(V)–V* plot of the junction. From Norde's functions, R_s value can be determined as;

$$R_s = \frac{kT(\gamma - n)}{qI}. \tag{10}$$

From the *F–V* plot by using $F(V_0) = 0.62$ V and $V_0 = 0.15$ V values, the values of Φ_b and R_s of the Au/CuO/p-Si MIS diode have been determined as 0.64 eV and $2.36 \times 10^3\ \Omega$, respectively. There is a difference in the values of Φ_b obtained from the forward bias ln *I–V*, Cheung functions and Norde functions. Differences in the barrier height values obtained from three methods for the device may be attributed to the extraction from different regions of the forward bias current–voltage plot [57]. However, the value of the series resistance obtained from Norde function is higher than that obtained from Cheung functions. Cheung functions are only applied to the nonlinear region in high voltage section of the forward bias ln *I–V* characteristics, while Norde's functions are applied to the full forward bias region of the ln *I–V* characteristics of the junctions [57]. The value of series resistance may also be large for the higher ideality factor values. Furthermore, the value of series resistance is very high for this device. This indicates that the series resistance is a current-limiting factor for this structure. The effect of the series resistance is usually modeled with series combination of a diode and a resistance R_s. The voltage drop across a diode is expressed in terms of the total voltage drop across the diode and the resistance R_s. The very high series resistance behavior may be ascribed to decrease of the exponentially increasing rate in current due to space-charge injection into the CuO thin film at higher forward bias voltage [57]. Furthermore, Norde's model may not be a suitable method especially for the high ideality factor of the rectifying junctions, which are non-agree with pure thermionic emission theory. Therefore, the series resistance value from Norde functions can be much higher than one from Cheung model for especially non-ideal rectifying structures [57].

3.3. Analysis of interfacial properties of the Au/CuO/p-Si MIS structure

For a MS diode having interface states in equilibrium with the semiconductor the ideality factor n becomes greater than unity as proposed by Card and Rhoderick [58] and then interface-state density N_{SS} is given by

$$N_{SS} = \frac{1}{q}\left[\frac{\varepsilon_i}{\delta}(n(V) - 1) - \frac{\varepsilon_s}{w}\right] \tag{11}$$

where w is the space charge width, ε_s is the permittivity of the semiconductor, ε_i is the permittivity of the interfacial layer, δ is the thickness of CuO interlayer, and $n(V) = V/((kT/q)\ln(I/I_0))$ is voltage-dependent ideality factor. In *p*-type semiconductors, the energy of the interface states E_{SS} with respect to the top of the valence band at the surface of the semiconductor is given by;

$$E_{SS} - E_V = q\Phi_b - qV \tag{12}$$

where V is the voltage drop across the depletion layer and Φ_b is the effective barrier height. The energy distribution or density distribution curves of the interface states can be determined from experimental data of this region of the forward bias *I–V* plot. Substituting the voltage-dependent values of n and the other parameters in Eq. (11), the N_{SS} *vs.* $E_{SS} - E_V$ plot was obtained as shown in Fig. 9. It is seen that N_{SS} value decreases with increasing $E_{SS} - E_V$ value. The density distribution of the interface states of the diode changes from 6.21×10^{12} to $1.62 \times 10^{12}\ \text{eV}^{-1}\ \text{cm}^{-2}$. Aydogan et al. [52] have found that the deposition of organic interlayers on to the

inorganic semiconductor could generate large number of interface states at the semiconductor surface, which strongly have influenced the properties of the PANI/p-Si/Al structure. Çakar et al. [59] have determined interface properties of Au/PYR-B/p-Si/Al contact. They [59] have found that the interface-state density values vary from 4.21×10^{13} to 3.82×10^{13} cm^{-2} eV^{-1}. In another study, Aydin and Türüt [60] have investigated the interface-state density properties of the Sn/methyl-red/p-Si/Al diode and interface-state density was found to vary from 1.68×10^{12} to 1.80×10^{12} cm^{-2} eV^{-1}. The interface-state density of the Au/CuO/p-Si MIS diode is consistent with those of above mentioned diodes. It is evaluated that interface properties of Au/p-Si junction are changed by depending on CuO interlayer inserted into the metal and the semiconductor. The CuO interlayer appears to cause to a significant modification of interface states even though the oxide-semiconductor interface appears abrupt and unreactive [61–63]. The CuO interlayer increases the effective barrier height clearly upon the modification of the semiconductor surfaces and the chemical interaction at the interface of the CuO to the p-Si and native oxide–CuO interface states will give rise to new interface states [43].

4. Conclusions

In summary, it was determined the best conditions for preparation of productive CuO nanofilms. CuO nanofilms were deposited on p-Si substrate by a spin-coating and annealing process. The CuO nanofilms were characterized by XRD, UV–vis spectroscopy, FT-IR spectroscopy and PL spectroscopy. Structural analysis results demonstrate that the single phase CuO on Si substrate is of high a crystalline structure with a dominant in monoclinic (1 1 1) orientation. FT-IR results confirm the formation of pure CuO phase. UV–vis absorption measurements indicated that the band gap of the CuO films is 2.64 eV. The PL spectrum of the CuO films shows a broad emission band centered at 467 nm, which is aggrement with absorption measurement. Also, the Au/CuO/p-Si MIS diodes have been fabricated. The current–voltage of these structures were studied. The ideality factor and barrier height of the MIS diode were obtained as 2.39 an 0.64 eV, respectively. The interface-state density of the MIS diode was found to vary from 6.21×10^{12} to 1.62×10^{12} eV^{-1} cm^{-2}.

Acknowledgments

The authors gratefully acknowledge financial supports from Bingöl, Batman, Atatürk and Sakarya Universities. Also, Dr. O. Gullu wish to thank Prof. Dr. A. Turut for his valuable helps and supports.

References

[1] M. Caglar, F. Yakuphanoglu, J. Phys. D: Appl. Phys. 42 (2009) 045102.
[2] C. Cantalini, J. Eur. Ceram. Soc. 24 (2004) 1421.
[3] A.Y. Oral, E. Mensur, M.H. Aslan, E. Basaran, Mater. Chem. Phys. 83 (2004) 140.
[4] U.D. Lanke, M. Vedawyas, Nucl. Inst. Methods Phys. Res. B 155 (1999) 97.
[5] S.C. Ray, Solar Energy Mater. Solar Cells 68 (2001) 307.
[6] T. Maruyama, Solar Energy Mater. Solar Cells 56 (1998) 85.
[7] S.M. Sze, Physics of Semiconductor Devices, second ed., Wiley, New York, 1981.
[8] P. Cova, A. Singh, Solid-State Electron. 33 (1990) 11.
[9] S. Karatas, S. Altındal, Solid-State Electron. 49 (2005) 1052.
[10] M.P. Houng, Y.H. Wang, N.F. Wang, W.J. Chang, C.I. Hung, Mater. Chem. Phys. 59 (1) (1999) 36.
[11] K.R. Rajesh, C.S. Menon, J. Non-Cryst. Solids 353 (4) (2007) 398.
[12] T. Kilicoglu, M.E. Aydin, Y.S. Ocak, Physica B 388 (1/2) (2007) 244.
[13] R. Balasundaraprabhu, E.V. Monakhov, N. Muthukumarasamy, O. Nilsen, B.G. Svensson, Mater. Chem. Phys. 114 (1) (2009) 425.
[14] R.K. Gupta, R.A. Singh, Mater. Chem. Phys. 86 (2004) 279.
[15] R.K. Gupta, K. Ghosh, P.K. Kahol, Physica E 41 (2009) 876.
[16] A.O. Abu-Hilal, A.M. Saleh, R.D. Gould, Mater. Chem. Phys. 94 (1) (2005) 165.
[17] P. Koteswara Rao, V. Rajagopal Reddy, Mater. Chem. Phys. 114 (2/3) (2009) 821.
[18] M.A. Ebeoglu, T. Kilicoglu, M.E. Aydin, Physica B 395 (2007) 93.
[19] D.P. Singh, A.K. Ojha, O.N. Srivastava, J. Phys. Chem. C 113 (2009) 3409.
[20] A.A. Dakhel, J. Alloys Compd. 476 (1/2) (2009) 28.
[21] C. Xu, Q. Xiao, J. Maa, Y. Jin, J. Shao, Z. Fan, Appl. Surf. Sci. 254 (2008) 6554.
[22] Y.T. Nien, I.G. Chen, J. Alloys Compd. 471 (1/2) (2009) 553.
[23] M. Deepa, M. Kar, S.A. Agnihotry, Thin Solid Films 468 (2004) 32.
[24] A.F. Qasrawi, J. Alloys Compd. 455 (1/2) (2008) 295.
[25] Y. Caglar, S. Ilican, M. Caglar, F. Yakuphanoglu, J. Wu, K. Gao, P. Lu, D.F. Xue, J. Alloys Compd. 481 (1/2) (2009) 885.
[26] V.R. Shinde, T.P. Gujar, C.D. Lokhande, R.S. Mane, S.H. Han, Appl. Surf. Sci. 250 (2005) 161.
[27] M.A. Dar, Y.S. Kim, W.B. Kim, J.M. Sohn, H.S. Shin, Appl. Surf. Sci. 254 (2008) 7477.
[28] B. Balamurugan, B.R. Mehta, Thin Solid Films 396 (2001) 90.
[29] K.P. Muthe, J.C. Vyas, S.N. Narang, D.K. Aswal, S.K. Gupta, D. Bhattacharya, R. Pinto, G.P. Kothiyal, S.C. Sabharwal, Thin Solid Films 324 (1998) 37.
[30] N.F. Mott, R.W. Gurney, Electronic Processes in Ionic Crystals, Oxford U. Press, London, 1940.
[31] A.K. Abass, A. Krier, R.A. Collins, Phys. Stat. Sol. (a) 142 (1994) 435.
[32] K.R. Rajesh, C.S. Menon, Eur. Phys. J. B 47 (2005) 171.
[33] O. Gullu, A. Turut, Solar Energy Mater. Solar Cells 92 (10) (2008) 1205.
[34] Q. Liu, H. Liu, Y. Liang, Z. Xu, G. Yin, Mater. Res. Bull. 41 (2006) 697.
[35] X. Zhang, D. Zhang, X. Ni, H. Zheng, Solid-State Electron. 52 (2008) 245.
[36] D.I. Son, C.H. You, T.W. Kim, Appl. Surf. Sci. 255 (2009) 8794.
[37] H. Wang, J.Z. Xu, J.J. Zhu, H.Y. Chen, J. Cryst. Growth 244 (2002) 88.
[38] E.H. Rhoderick, R.H. Williams, Metal—Semiconductor Contacts, 2nd ed., Clarendon, Oxford, 1988.
[39] R.F. Schmitsdorf, T.U. Kampen, W. Monch, J. Vac. Sci. Technol. B 15 (4) (1997) 1221.
[40] W. Monch, J. Vac. Sci. Technol. B 17 (4) (1999) 1867.
[41] R.T. Tung, Phys. Rev. B 45 (23) (1992) 13509.
[42] G.M. Vanalme, L. Goubert, R.L. Van Meirhaeghe, F. Cardon, P. Van Daele, Semicond. Sci. Technol. 14 (1999) 871.
[43] F. Yakuphanoglu, M. Kandaz, B.F. Senkal, Thin Solid Films 516 (2008) 8793.
[44] C. Temirci, M. Çakar, Physica B 348 (2004) 454.
[45] Ş. Karatas, C. Temirci, M. Çakar, A. Türüt, Appl. Surf. Sci. 252 (2006) 2209.
[46] M. Çakar, C. Temirci, A. Türüt, Synth. Met. 142 (2004) 177.
[47] M. Çakar, Y. Onganer, A. Türüt, Synth. Met. 126 (2002) 213.
[48] T. Kampen, A. Schuller, D.R.T. Zahn, B. Biel, J. Ortega, R. Perez, F. Flores, Appl. Surf. Sci. 234 (2004) 341.
[49] A.R.V. Roberts, D.A. Evans, Appl. Phys. Lett. 86 (2005) 072105.
[50] A. Bolognesi, A. Di Carlo, P. Lugli, T. Kampen, D.R.T. Zahn, J. Phys. Condens. Mat. 15 (2003) S2719.
[51] D.R.T. Zahn, T.U. Kampen, H. Mendez, Appl. Surf. Sci. 212 (2003) 423.
[52] S. Aydogan, M. Saglam, A. Turut, Microelectron. Eng. 85 (2008) 278.
[53] A. Turut, M. Saglam, H. Efeoglu, N. Yalcin, M. Yildirim, B. Abay, Physica B 205 (1995) 41.
[54] S.K. Cheung, N.W. Cheung, Appl. Phys. Lett. 49 (1986) 85.
[55] T. Kilicoglu, Thin Solid Films 516 (2008) 967.
[56] S. Karatas, S. Altindal, A. Turut, M. Cakar, Physica B 392 (1/2) (2007) 43.
[57] O. Gullu, S. Aydogan, A. Turut, Microelectron. Eng. 85 (2008) 1647.
[58] H.C. Card, E.H. Rhoderick, J. Phys. D 4 (1971) 1589.
[59] M. Çakar, N. Yıldırım, H. Doğan, A. Türüt, Appl. Surf. Sci. 253 (2007) 3464.
[60] M.E. Aydın, A. Türüt, Microelectron. Eng. 84 (2007) 2875.
[61] T.U. Kampen, S. Park, D.R.T. Zahn, Appl. Surf. Sci. 190 (2002) 461.
[62] M. Cakar, N. Yildirim, S. Karatas, C. Temirci, A. Turut, J. Appl. Phys. 100 (2006) 074505.
[63] S.R. Forrest, M.L. Kaplan, P.H. Schmidt, J. Appl. Phys. 60 (1986) 2406.